Anisotropic field-induced melting of orbital ordered structure in $Pr_{0.6}Ca_{0.4}MnO_3$

Huali Yang,[1] Yiwei Liu,[1] Jiandi Zhang,[2,*] Xiangqun Zhang,[3] Zhaohua Cheng,[3] Yali Xie,[1] Baomin Wang,[1] Qingfeng Zhan,[1] B. G. Shen,[3] E. W. Plummer,[2] and Run-Wei Li[1,†]

[1]*Key Lab of Magnetic Materials and Devices, Ningbo Institute of Materials Technology and Engineering, Chinese Academy of Sciences, Ningbo 315201, Peoples Republic of China*

[2]*Department of Physics and Astronomy, Louisiana State University, Baton Rouge, Louisiana 70803, USA*

[3]*Beijing National Laboratory for Condensed Matter Physics and Institute of Physics, Chinese Academy of Sciences, Beijing 100190, Peoples Republic of China*

(Received 8 September 2014; revised manuscript received 18 April 2015; published 6 May 2015)

The magnetic field-dependent transport of $Pr_{0.6}Ca_{0.4}MnO_3$ has been investigated to expose the field-induced melting of orbital ordering. The critical field and critical temperature for the melting of the orbital ordered state depend on the orientation of the applied magnetic field, seemingly independent of the nature of the magnetic phase. The crystalline c axis is the hard axis of the field-induced melting, but in-plane anisotropy also exists, correlating with the anisotropic charge-exchange-(CE) type orbital-ordered structure. These findings demonstrate that the anisotropic melting coincides with the orbital ordering anisotropy, thus indicating a strong spin-orbital coupling.

DOI: 10.1103/PhysRevB.91.174405 PACS number(s): 71.30.+h, 73.22.Gk, 75.47.Gk

I. INTRODUCTION

In many transition metal oxides (TMOs), the exhibited functionality is closely related to the synergetic interactions between simultaneously active degrees of freedom—charge, lattice, orbital, and spin. One intriguing phenomenon is orbital ordering observed in several TMOs [1] (such as perovskite manganites) in which the antiferromagnetic insulating (AFI) state is normally accompanied by the orbital ordered (OO) phase. The AFI-OO phase can be thermally driven either into an orbital-liquid and ferromagnetic metallic (FMM) state or directly into a paramagnetic insulating phase (PMI), depending on doping concentration [2]. In the latter case, the antiferromagnetic (AF) to paramagnetic (PM) transition may occur at lower temperature (T) than the OO phase transition [3,4]. The insulating OO phase can also be destroyed by a magnetic field, resulting in a concurrent first-order field-induced melting of OO state and metal-insulator transition (MIT) [5,6]. The occurrences of these phase transitions indicate an unusual spin-orbital interaction [1], but currently it is unclear how the magnetic field causes the melting. Presumably, the application of magnetic field tends to align the Mn t_{2g} spins, which leads to an increase in the transfer integral of e_g electrons between Mn^{3+} and Mn^{4+} ions through double exchange interaction. Once the kinetic energy of the charge carriers dominates over the OO instability, the field-induced destruction of OO takes place [7]. The above mechanism that accounts for the magnetic field-induced melting of OO seems to be only relevant to the spin exchange interaction which does not necessarily involve spin-orbital coupling. Experimentally, it is evident that the formation of OO state induces an anisotropic optical electronic transition [8,9]. Hence, it is speculated that the orbital degree of freedom effectively controls the interplay between double-exchange and superexchange interactions such that it has an intimate relationship to both charge and spin dynamics in the system. However, how spin-orbital coupling manifests itself in the formation of OO state and the field-induced melting is still unclear.

In this article we report the observation of anisotropic behavior of field-induced melting of the OO state, as a function of field and temperature, in a prototype manganite $Pr_{1-x}Ca_xMnO_3$ ($x = 0.4$), especially above the Néel temperature (T_N). The critical temperature and critical field for melting the OO state depend on the orientation of the applied magnetic field, independent of the nature of the magnetic phase. These results provide experimental evidence reflecting the broken symmetry of the OO superstructure, and the involvement of spin-orbital coupling in the magnetic field-induced OO melting process is also confirmed.

Figure 1(a) displays the crystal structure of these three-dimensional perovskites, $R_{1-x}A_xMnO_3$ (R = trivalent rare-earth ion; A = alkali earth ions). In this study R is Pr and A is Ca. Ideally the structure would be simple cubic but Jahn-Teller distortions reduce symmetry by transforming simple cubic to orthorhombic structure, such that one of the Mn-O bond lengths in the basic building block of MnO_6 octahedron is different than the other two in the MnO_2 basal plane (i.e., ab plane). Given the existence of anisotropic crystal structure, a two-dimensional CE-type layered OO state is often observed in these materials, as shown in Fig. 1(b). Based upon the conventional picture [10] for half-doped narrow-bandwidth manganites ($x = 0.5$), nominally Mn^{3+} and Mn^{4+} ions occupy alternative lattice sites forming a checkerboard pattern in the MnO_2 basal planes [the ab plane in Figs. 1(b) and 1(d)]. A staggered ordering of the nominal Mn^{3+} electron between the two e_g orbitals ($d_{3x^2-r^2}$ and $d_{3y^2-r^2}$) corresponds to the wave vector ($\pi, \pi, 0$) in the pseudocubic notation [3,4,10]. Such a CE-type orbital ordering also persists in the manganites away from the half-doping region ($x < 0.5$) [6,11–15], resulting in either a Mn^{3+}/Mn^{4+} charge-ordered but phase-separated ground state or a charge-disproportionated homogeneous OO ground state. In the latter scenario, the possible charge order is described as alternating $Mn^{3.5+\delta}$ and $Mn^{3.5-\delta}$ structure where δ denotes the amount of charge disproportionation in Mn

*jiandiz@lsu.edu
†runweili@nimte.ac.cn

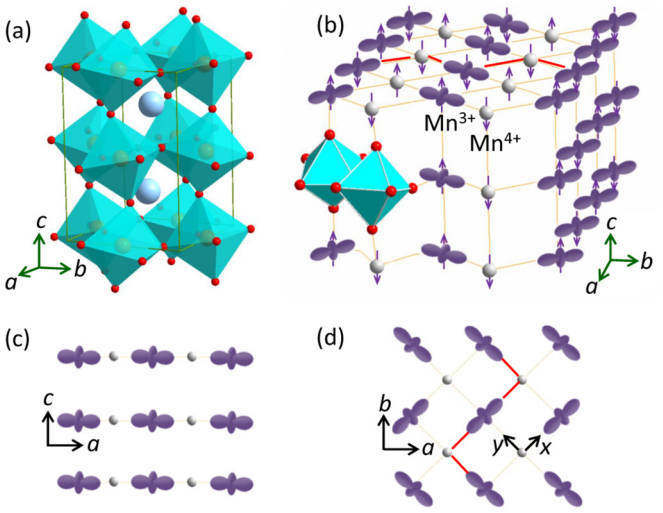

FIG. 1. (Color online) (a) Model of the orthorhombic crystal structure of $Pr_{0.6}Ca_{0.4}MnO_3$, where the MnO_6 octahedra are presented. (b) Schematic spin and orbital structure in the ideal AFM CE-type OO state, where the ordered e_g orbital lobes associated with the Mn^{3+} ions are shown in contrast to the Mn^{4+} ions (light gray spheres). (c) Side and (d) top view of e_g-orbital ordering. The thick zigzag lines represent double-exchange interaction chains.

valence [13]. In $Pr_{0.6}Ca_{0.4}MnO_3$, the charge order is believed to drive OO below T_{OO} [4], and applying a magnetic field will destroy the charge order along with OO [16].

Spin and orbital ordering in the CE-type OO state exhibits anisotropic behavior within the *ab* plane as well as along the *c* axis [3,4,10]. In the CE-type OO state, the e_g orbitals lie in the *ab* plane, thus having an in- and out-of-plane anisotropy [Fig. 1(c)]. The e_g orbital shows a striped behavior along the *a* axis but a zigzag chain behavior along the *b* axis of the *ab* plane, as shown in Fig. 1(d). In the orthorhombic unit cell notation this results in additional in-plane anisotropy with reduced C_{2V} symmetry. Below the Néel temperature T_N, which is usually lower than the OO transition temperature T_{OO}, the spins of localized t_{2g} orbitals at Mn sites are ordered ferromagnetically along the zigzag chain path (along the *b* axis) but antiferromagnetically between the chains (along the *a* axis), thus forming a globally AFI state in-plane [Fig. 1(b)]. In the AFI-OO state the spins are aligned parallel or antiparallel to the *c* axis. But as the temperature is lowered the spins exhibit gradually canting towards the *b* axis and eventually form a long-range canted antiferromagnetic magnetic ordering with the same OO structure as in the AFI-OO phase, thus referred to as the CAFI-OO phase [17]. Whether spin ordering in the ground state is AFI or CAFI depends on the doping level [6]. One can anticipate that, if there is a strong coupling between spin and orbital degrees of freedom, such an OO superstructure should give rise to the anisotropy of the electron-transfer interaction, thus resulting in anisotropic transport responses to the external field.

$Pr_{1-x}Ca_xMnO_3$ exhibits different OO ground states for a wide doping range ($0.3 < x < 0.7$) [18]. For the purpose of this study, a homogeneous OO state is preferred, therefore the best doping level would be $x = 0.5$. However, the magnetic field required to melt the OO state in the $x = 0.5$ sample is higher than 20 T [7], thus it is technically difficult to conduct the magnetotransport experiments. Fortunately, it has been demonstrated by neutron diffraction that the $x = 0.4$ sample, which has a lower critical field for the melting, exhibits a homogeneous CAFI-OO ground state described as a charge disproportionation scenario [6,15]. Given the similarities between the CAFI-OO and AFI-OO phases we can expect no phase separation in the AFI-OO phase. $Pr_{0.6}Ca_{0.4}MnO_3$ exhibits orthorhombic structure at room temperature [Fig. 1(a)]. By lowering the temperature, the CE-type OO state sets in, and the lattice experiences a structural transition across T_{OO} by reducing the lattice constant the in *c* axis while increasing those in the *ab* plane [17] but no change in symmetry.

II. EXPERIMENTAL DETAILS

The single crystal of $Pr_{0.6}Ca_{0.4}MnO_3$ investigated here was grown by the floating-zone method. Polycrystalline samples with nominal composition of $Pr_{0.6}Ca_{0.4}MnO_3$ were prepared by the solid state reaction method. The as-grown single phase powders were then hydrostatically pressed into feed and seed rods that were sintered at 1450 °C for 48 h. The crystal growth was carried out in an optical floating-zone furnace (Crystal Systems Inc., ZT-10000-H-VI-VP) equipped with four 1000 W halogen lamps and ellipsoidal mirrors. A single crystal was grown with 80% power supply under 1 atm oxygen pressure. The rods rotated at 25 rpm in opposite directions, and the typical growth rate was 3 mm/h.

The crystal structure was characterized with x-ray diffraction. The crystal was confirmed having a single phase of distorted perovskite with a *Pbnm* orthorhombic lattice structure. The as-grown crystal has twinned microstructures which were characterized with both Laue and synchrotron x-ray diffractions (the detailed results are described in the Supplemental Material [19]). First, back-reflection Laue x-ray diffraction was carried out to determine the crystallographic direction of the sample. Laue diffraction patterns showed no significant twinning between the *c* axis and *ab* plane. However, due to the small lattice contrast between *a* and *b*, severe twinning exists in the *ab* plane so that it is hard to distinguish the *a* axis from the *b* axis. We have performed synchrotron x-ray diffraction (BL14B at Shanghai Synchrotron Radiation Facility, SSRF), and significant twinning in the *ab* plane was further confirmed.

The transport and magnetotransport were carried out with a Physical Property Measurement System (PPMS, Quantum Design) equipped with a motorized sample rotator and a standard four-probe contact for the resistivity measurements. During measurement, the magnetic field (H) is rotated within the plane that is always perpendicular to the current flow direction, so any changes observed cannot be attributed to changes in the strength of the Lorentz force. T-dependent magnetization was measured by using a Magnetic Property Measurement System (MPMS, Quantum Design).

III. RESULTS AND DISCUSSION

Figure 2(a) shows the T dependence of the resistivity and magnetization, which is consistent with reported results [20–22]. The resistivity with zero-field cooling shows a jump

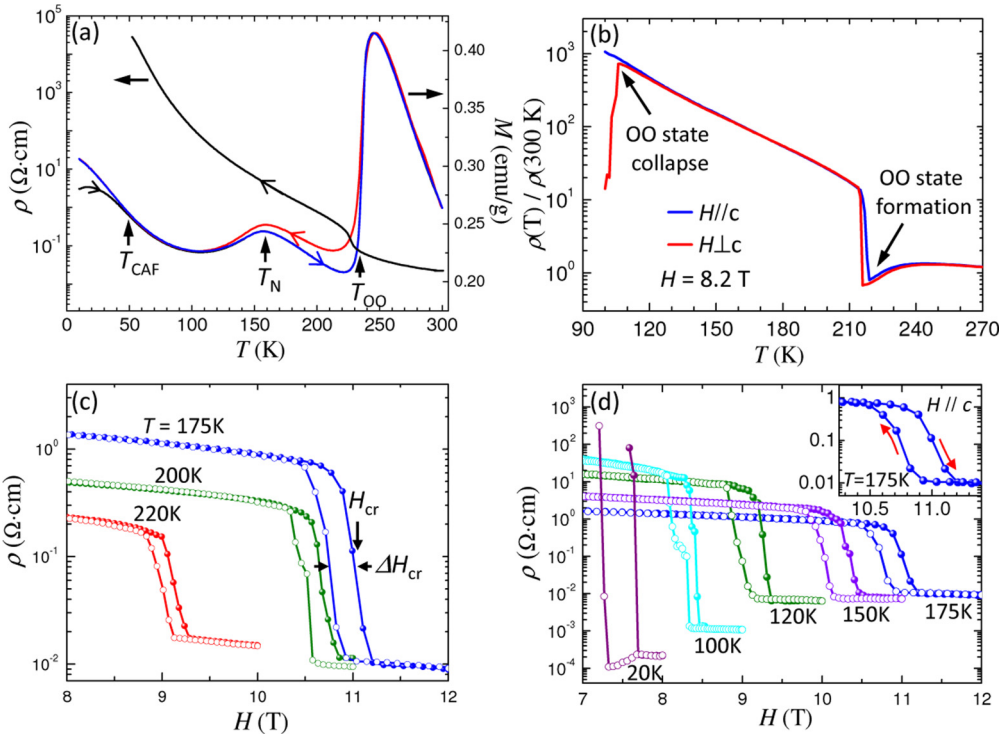

FIG. 2. (Color online) (a) T dependence of the resistivity (zero-field cooling) and magnetization of $Pr_{0.6}Ca_{0.4}MnO_3$ under $H = 0.1$ T (applied in the ab plane) showing thermal hysteresis (red and blue curves) measured after field cooling compared with that after zero-field cooling (black curve which merges with blue one above 49 K). T_{OO} and T_N are indicated, respectively. (b) Normalized (to $T = 300$ K) T dependence of the resistivity(on cooling) with H (8.2 T) $\parallel$ and $\perp$ c axis, respectively. Isothermal magnetoresistivity with increasing magnetic field along the c axis and in the ab plane, respectively, for the selected temperatures (c) above and (d) below $T = 175$ K. Both the critical field H_{cr} (defined as the field value with the maximum of $\frac{d\rho}{dH}$) and the difference of the critical field between $H \parallel$ and $\perp$ c axis (ΔH_{cr}) are indicated with arrows. The inset presents the resistivity hysteresis between field increasing and decreasing near the critical field range at $T = 175$ K. The current (I) for the resistivity measurement is always perpendicular to the field direction.

as the OO state emerges below $T_{OO} \cong 235$ K, then steadily increases with further decreasing temperature and exceeds the limit of our measurement below 56 K. The magnetization measurements also show response to OO transition at T_{OO} as well as AFI transition at $T_N \cong 160$ K and CAFI transition at $T_{CAF} \sim 49$ K. Thermal hysteresis exhibited in the magnetization curves indicates the first-order character of the OO transition. When in PMI phase ($T > T_{OO}$), the magnetization (or magnetic susceptibility which exhibits Curie-Weiss behavior) is driven by FM correlations. Due to the existence of double-exchange interaction, such FM correlations persist at lower temperatures, which can be seen in the subsequent increase in the magnetization curve. On the other hand, the AF correlation, which is favored in the OO phase, prevails below T_N and results in long-range AF ordering. The competition between FM and AF correlations leads to different magnetic structures and strongly depends on the doping concentration. For $Pr_{0.6}Ca_{0.4}MnO_3$, the gap between T_{OO} and T_N is ~75 K, thus providing a large temperature window for studying the anisotropic field response from OO state without long-range magnetic ordering.

Figure 2(b) presents the normalized T-dependent resistivity for field cooling with a magnetic field of $H = 8.2$ T applied along the c axis and in the ab plane. The abrupt increase of resistivity near 220 K indicates the formation of the OO state, showing lower OO transition temperature on field cooling than zero-field cooling [Fig. 2(a)]. Moreover, there is a small difference in the onset temperature of the OO state with different field orientations. With further field cooling, the resistivity shows a sudden drop below 107 K signifying the collapse of the OO state, but only for the case where H is applied in the ab plane. There is no trace of field-induced collapse of the OO state down to 100 K for the field applied along the c axis. This shows unambiguously a field orientation dependent melting of the OO state.

We have carried out a set of isothermal magnetoresistance (MR) measurements at different temperatures. In order to avoid the hysteresis issue, we cooled the sample from room temperature at zero field and then performed the field-dependent measurements at a fixed temperature. The sample was always brought up to room temperature before performing different isothermal MR measurements. Figure 2(c) displays several isothermal MR curves with $H \parallel c$ axis and $H \parallel ab$ plane, all above T_N. When $H \parallel c$ axis the curves for $T = 220$ K show that the OO state melts at a field of $H_{cr} \sim 9.2$ T, while the transition occurs at 10.7 T for 200 K and 11.2 T for 175 K. The critical field H_{cr} is always lower for fields in the ab plane, thus exhibiting melting anisotropy, regardless of the fact that the system has no long-range spin ordering.

We observed that the critical field for OO melting reaches its maximum value at $T \sim 175$ K and gradually decreases at lower temperatures as shown in Fig. 2(d). The isothermal

MR curves for $T = 175$ K is repeated in Fig. 2(d) to set the scale. The curves for $T = 150$ and 120 K show that H_{cr} has fallen to ∼10.4, and to 9.3 T, respectively, for $H \parallel c$ axis. It is worthwhile to note that the base resistivity after the melting is very similar for temperatures from 200 to 120 K but drops significantly below 120 K (two orders of magnitude for 20 K compared to 120 K) and the step of resistivity change across the melting increases dramatically. At 20 K and in the CAFI-OO state, the height of the step of resistivity change is at least 5 orders of magnitude larger than that at 175 K and the difference of the critical fields between the two field directions (ΔH_{cr}) is also larger. The reduction in base resistivity is a result of the appearance of FMM state at low temperatures and high fields. The fact that the anisotropic behavior is larger in the CAFI-OO state is counterintuitive, since canting of the spins in Fig. 1(b) should reduce the anisotropic behavior. Furthermore, there is hysteresis between field increasing and field decreasing at all measured temperatures below T_{OO} (see the inset for $T =$ 175 K), indicating the first-order character of the field-induced melting [5].

With the data presented in Figs. 2(c) and 2(d) we can plot the phase diagram of the OO melting as a function of temperature and magnetic field [see Fig. 3(a)]. This type of phase diagram has been reported previously [6,21], but our emphasis is the anisotropic behavior exhibited as a function of the direction of the magnetic field, and the magnetic state. Given the large hysteresis in this system it is essential to only compare our data with equivalent field-increasing experiments. As the magnetic field increases there is a slight decrease in T_{OO} from ∼235 K at $H = 0$ T to ∼200 K at 10 T [7]. The OO state cannot exist for a field greater than ∼11 T independent of the direction of the magnetic field. If this was a simple phase diagram between AFI-OO phase and PMI phase there would probably be nothing of interest happening at lower temperatures after the field was high enough to melt the OO structure, but the PMI phase transfers directly to a FMM phase with increasing field and decreasing temperature [6,21]. However, it is not clear where this boundary is in the phase diagram. The dotted region in Fig. 3(a) is what one would extract from the literature, but our data for the resistivity above and below the OO transition indicate a dramatic conductivity change in the region of 100 K for field-increasing experiments [Fig. 2(d)].

It is evident from the phase diagram that there is an expansion of the FMM phase into the AFI-OO phase as the temperature is lowered [6]. What is really strange is that the phase boundary in the CAFI-OO region ($T < T_{CAF}$) turns back, with the critical field increasing with decreasing temperature. However, such "reentrant" behavior does not occur in the case of field decreasing, leaving a giant hysteresis between field-decreasing and field-increasing measurements [5,6,21]. The boundary between CAFI-OO and FMM phase for field decreasing follows the slope of the boundary in the higher temperature region as sketched by the dashed line in Fig. 3(a) [6]. Tomioka *et al.* [6] point out that this

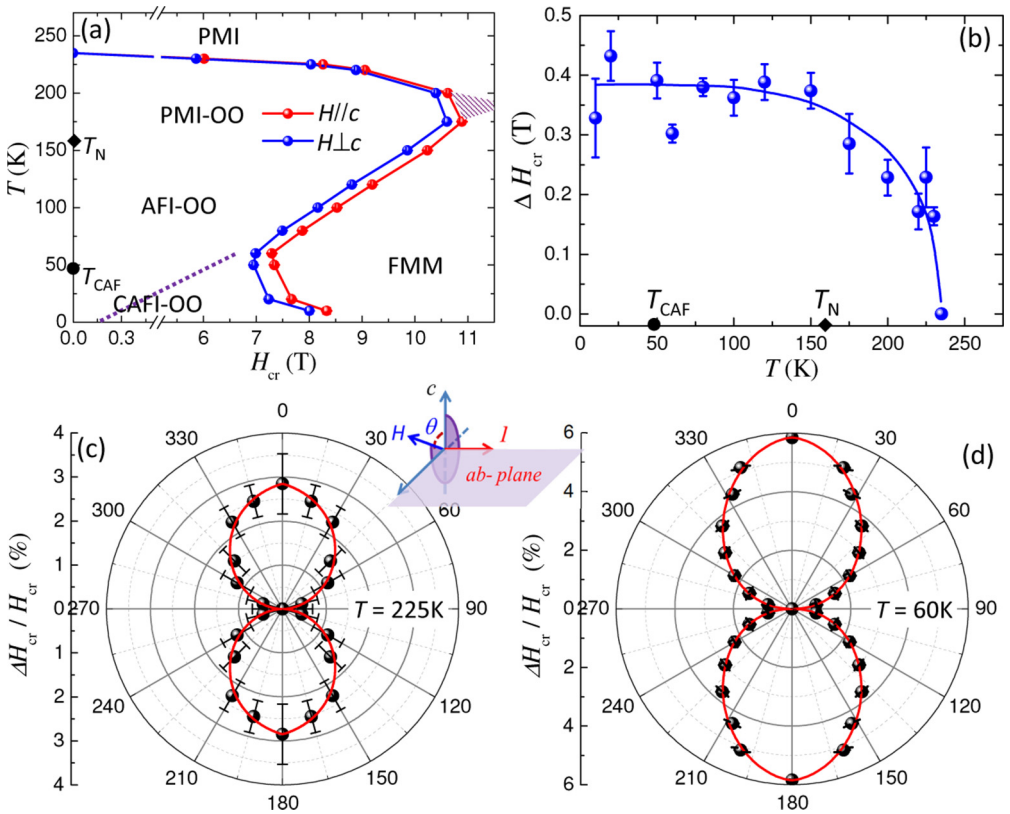

FIG. 3. (Color online) (a) Phase diagram showing the magnetic field orientation dependent melting of the OO state (from ordered to disordered transition) of $Pr_{0.6}Ca_{0.4}MnO_3$. The dashed line indicates the boundary from disordered to OO transition with decreasing field and the shaded area sketches PMI-FMM boundary under high field. (b) T dependence of ΔH_{cr}. The solid curve is a guide to the eye. Symmetrized plot of the normalized ΔH_{cr} (see the definition in the text) at (c) $T = 225$ K and (d) $T = 60$ K, respectively, based on the experimental data taken with $0^\circ < \theta < 90^\circ$. The inset shows the experimental configuration.

could be a result of the decrease in thermal fluctuations in the first-order phase transition. In fact, the hysteresis between field-decreasing and field-increasing measurements becomes much more dramatic in the CAFI-OO region [6,21].

The T dependence of $\Delta H_{cr}(T)$ is depicted in Fig. 3(b). $\Delta H_{cr}(T)$, which reflects the anisotropy of the field-induced OO melting, seems to be independent of the nature of the magnetic ordering in the OO phase. Only above T_N does the anisotropy start to decrease and eventually disappear as T approaches T_{OO}. In order to show more clearly such anisotropy, we plot the angle dependence of the normalized ΔH_{cr} (i.e., $\frac{\Delta H_{cr}}{H_{cr}} \times 100\% \equiv \frac{H_{cr}(\theta)-H_{cr}(\theta=\pi/2)}{H_{cr}(\theta=\pi/2)} \times 100\%$) for two temperatures, $T = 225$ K above T_N in Fig. 3(c) and $T = 60$ K below T_N in Fig. 3(d), respectively. The angle θ is defined as the angle between applied field direction and the c axis of the crystal (see the inset of Fig. 3). Clearly the anisotropy of the field-induced melting is qualitatively identical below and above T_N, which is very strange behavior.

Given the in-plane CE-type OO structure shown in Fig. 1(d), one would also expect to observe in-plane angular dependent MR. We have indeed observed in-plane anisotropy in the OO state melting although weaker than the out-of-plane one. Figure 4(a) shows a small difference in critical field H_{cr} between $\phi = 0^\circ$ and 90° observed at $T = 225$ K, where ϕ is defined as the in-plane rotation angle between H and one of the in-plane high-symmetry directions of the crystal. [Due to the severe twinning in the ab plane, we are unable to clearly distinguish the a from b axis of the crystal. Therefore, the $a(b)/b(a)$ axis is defined as the direction in which the a/b axis of majority of twinning domains aligns.] The angular dependent MR at $T = 225$ K with different field values close to in-plane H_{cr} is also measured and displayed in Fig. 4(b). At a field close to 7.65 T, there is irreversible resistivity drop with rotating the magnetic field, signifying the melting of the OO state. As the magnetic field value deviates away from the critical field one (such as $H = 7.0$ or 9.0 T), ordinary oscillatory angular dependent MR behavior is observed [23]. We anticipate that the twining in the ab plane (see the Supplemental Material [19]) would average out much of the in-plane anisotropy. What we observed in the isothermal MR curves [Fig. 4(a)] reflects the residual anisotropy only. However, due to the first-order nature of the OO melting, the twining exhibited in the ab plane actually does not affect our observation of anisotropic melting behavior from the angular dependent MR measurements. Similar in-plane anisotropy of the electronic response has been observed with optical conductivity spectroscopy in a half-doped manganite with layered structure [9,24]. Nevertheless, both in-plane and out-of-plane anisotropy exist in the system, correlated with the anisotropy of the CE-type OO structure.

Several mechanisms for the formation of OO state have been proposed, including anisotropic exchange interactions [13,25], strong electron correlation [26,27], and cooperative Jahn-Teller type interactions [4,12]. One can anticipate that the transport strongly depends on the exchange interactions which are subject to both spin and orbital orientation between different Mn ions [1,28]. Applying an external field to the system should affect these exchange interactions by altering the relative orientation between spins and orbitals, thus resulting in magnetoresistance effect including field-induced melting of the OO state [29]. Hence, a magnetic ordered OO state is expected to exhibit larger melting anisotropy than its nonmagnetic counterparts.

In our case, the melting anisotropy persists in both AFI-OO and PMI-OO phases. There is no difference in melting anisotropy across T_N [see Fig. 3(b)]. The T dependence of ΔH_{cr} resembles the orbital order parameter [4] rather than the AF order parameter. It does not seem to be sensitive to the presence of any specific magnetic order. In the temperature region $T_N < T < T_{OO}$, it is believed that short-range FM spin correlations and antiferromagnetic spin interaction compete with each other, and result in a very strange paramagnetic spin state. However, such short-range FM correlations or fluctuations show strong doping and temperature dependence. According to the results of neutron scattering [15,30], as the doping level is larger than 0.35, the FM fluctuations are strong in PM phase and then dramatically suppressed below T_{OO} and vanish below T_N. Furthermore, the measured magnetic susceptibility of $Pr_{0.6}Ca_{0.4}MnO_3$ shows no anisotropy above T_N [22,31]. Hence the FM fluctuations cannot be the driving force for the anisotropic melting.

One possible explanation for the appearance of field-induced melting anisotropy without anisotropic magnetic ordering ($T > T_N$ case) comes from the strong spin-orbital

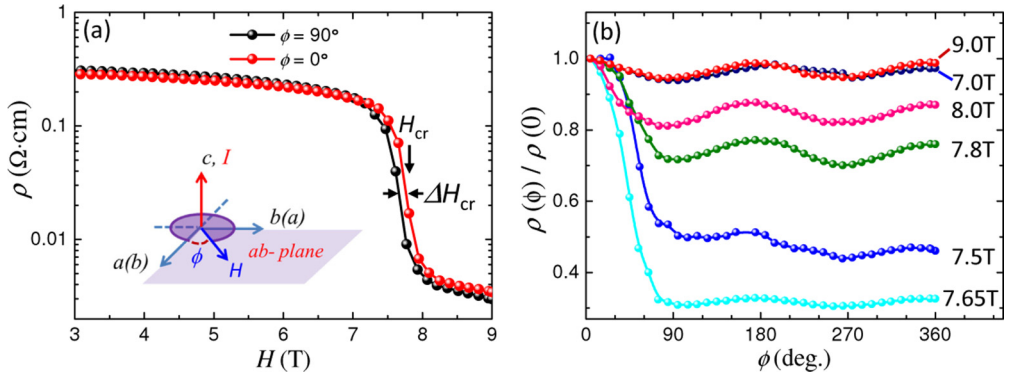

FIG. 4. (Color online) (a) Field dependence of the isothermal ($T = 225$ K) resistivity with $\phi = 0^\circ$ and 90°, respectively. Inset shows the experimental configuration. (b) Angle dependence of the MR curves at 225 K with different values of the applied magnetic field. The critical field H_{cr} and difference (ΔH_{cr}) are marked by the arrows.

interaction. According to the generalized Heisenberg-type model with spin-orbital exchange interaction [1,28], the formation of OO state can be described by a phenomenological Hamiltonian which represents the interactions between different ions: $H = \sum_{i,j}[J_{ij}(\mathbf{T_i},\mathbf{T_j})\,\mathbf{S_i}\cdot\mathbf{S_j} + K_{ij}(\mathbf{T_i},\mathbf{T_j})]$, where J_{ij} and K_{ij} are the exchange interactions [28]. The pseudospin ($\mathbf{T}$) represents orbital orientation similar to spin ($\mathbf{S}$) representing magnetic moment orientation. In this way, one can consider a long-range OO state of the orbital pseudospin $\mathbf{T}$ as a long-range magnetic ordered state of spin $\mathbf{S}$, thus the field-induced melting of OO state can be treated as a field-induced change of magnetic ordered state, due to the strong coupling between the spin $\mathbf{S}$ and pseudospin $\mathbf{T}$. Any anisotropy in an OO state will generate anisotropy in the melting of itself because the coupling depends on the orientation of $\mathbf{T}$. This seems to account for the field-induced melting as well as the associated anisotropy even without magnetic ordering or magnetic anisotropy.

Another possible contribution to the observed anisotropy is magnetoelastic effect, which cannot be completely excluded in our data. In manganites, magnetoelastic effects due to spin-lattice coupling result in measurable phenomena including transport responses. A remarkable anisotropic magnetotransport between in- and out-of-plane has been observed in orthorhombic $La_{1-x}Ca_xMnO_3$ due to anisotropic magnetoelastic response to external field [23]. Indeed, the twofold oscillatory MR behavior vs ϕ [see $\rho(\phi)/\rho(0)$ in Fig. 4(b) for $H = 7.0$, 7.8, 8.0, and 9.0 T] for the applied field far below or above the critical value (H_{cr}) should be related to the magnetoelastic effect similar to these observed in $La_{1-x}Ca_xMnO_3$ [23]. As a result of the intimate coupling between orbital occupation and lattice distortion, it is very difficult to convincingly deconvolve the effects of the anisotropic crystal structure from that of orbital ordering. In the measured temperature range (in both LT OO phase and RT orbital disordered phase), the system is in the same orthorhombic structure with crystalline anisotropy, thus it could be the cause for the melting anisotropy of OO phase. On the other hand, given the measured lattice constants at zero field for both the high-T orbital liquid phase ($a = 5.4155$ Å, $b = 5.4325$ Å, and $c = 7.6423$ Å at $T = 280$ K) and low-T OO phase ($a = 5.4310$ Å, $b = 5.4417$ Å, and $c = 7.6022$ Å at $T = 200$ K) [17], the in-plane orthorhombicity ($\varepsilon \equiv |\frac{a-b}{a+b}| \times 100\% = 0.16\%$ at 280 K and 0.10% at 200 K) is smaller though the unit cell is more compressed along the c axis ($\gamma \equiv \frac{c/\sqrt{2}}{(a+b)/2} = 0.9963$ at 280 K and 0.9888 at 200 K) in the OO phase. Therefore, it seems unlikely that the lattice anisotropy would be the primary driving force for the observed anisotropy of field-induced OO state melting. However, as a result of the strong coupling between orbital and lattice, we cannot rule out the effects of crystalline anisotropy.

IV. CONCLUSIONS

In summary, we have observed crystalline orientation dependence in the magnetic field-induced melting of the OO state in $Pr_{0.6}Ca_{0.4}MnO_3$ single crystals. The anisotropy of the field-induced melting is irrelevant to the magnetic structure but coincides with the anisotropy of OO structure. We explain the melting anisotropy based on the anisotropic spin-orbital coupling due to the anisotropic OO structure, though the orthorhombic crystalline anisotropy is also involved owing to the nature of the strong correlation between spin, lattice, and orbital degrees of freedom.

ACKNOWLEDGMENTS

We thank Jinglan Chen and Guangheng Wu for determining the crystallographic orientation of $Pr_{0.6}Ca_{0.4}MnO_3$ single crystals. We thank Xiaolong Li for performing the x-ray diffraction at Shanghai Synchrotron Radiation Facility. We are grateful to Wei Ku and Guo-Qiang Liu for helpful discussions. The financial support from State Key Project of Fundamental Research of China (973 Program, 2012CB933004, 2011CB921801), National Natural Science Foundation of China (11274321, 11174302, 11274360) are acknowledged. J.Z. is partially supported by U.S. NSF DMR-1005562.

[1] Y. Tokura and N. Nagaosa, Science **288**, 462 (2000).
[2] For a review, see, for example, Y. Tokura, ed., *Colossal Magnetoresistive Oxides* (Gordon and Breach, Tokyo, 1999).
[3] Y. Murakami, H. Kawada, H. Kawata, M. Tanaka, T. Arima, Y. Moritomo, and Y. Tokura, Phys. Rev. Lett. **80**, 1932 (1998).
[4] M. v. Zimmermann, J. P. Hill, D. Gibbs, M. Blume, D. Casa, B. Keimer, Y. Murakami, Y. Tomioka, and Y. Tokura, Phys. Rev. Lett. **83**, 4872 (1998).
[5] H. Kuwahara, Y. Tomioka, A. Asamitsu, Y. Moritomo, and Y. Tokura, Science **270**, 961 (1995).
[6] Y. Tomioka, A. Asamitsu, H. Kuwahara, Y. Moritomo, and Y. Tokura, Phys. Rev. B **53**, R1689(R) (1996).
[7] M. Tokunaga, N. Miura, Y. Tomioka, and Y. Tokura, Phys. Rev. B **57**, 5259 (1998).
[8] T. Ishikawa, K. Ookura, and Y. Tokura, Phys. Rev. B **59**, 8367 (1999).
[9] Y. S. Lee, S. Onoda, T. Arima, Y. Tokunaga, J. P. He, Y. Kaneko, N. Nagaosa, and Y. Tokura, Phys. Rev. Lett. **97**, 077203 (2006).
[10] J. B. Goodenough, Phys. Rev. **100**, 564 (1955).
[11] S. Grenier, J. P. Hill, D. Gibbs, K. J. Thomas, M. V. Zimmermann, C. S. Nelson, V. Kiryukhin, Y. Tokura, Y. Tomioka, D. Casa, T. Gog, and C. Venkataraman, Phys. Rev. B **69**, 134419 (2004).
[12] Ch. Jooss, L. Wu, T. Beetz, R. F. Klie, M. Beleggia, M. A. Schofield, S. Schramm, J. Hoffmann, and Y. Zhu, Proc. Natl. Acad. Sci. USA **104**, 13597 (2007).
[13] J. van den Brink, G. Khaliullin, and D. Khomskii, Phys. Rev. Lett. **83**, 5118 (1999).
[14] Z. Popovic and S. Satpathy, Phys. Rev. Lett. **88**, 197201 (2002).
[15] H. Sha, F. Ye, P. Dai, J. A. Fernandez-Baca, D. Mesa, J. W. Lynn, Y. Tomioka, Y. Tokura, and J. Zhang, Phys. Rev. B **78**, 052410 (2008).

[16] M. V. Zimmermann, C. S. Nelson, J. P. Hill, D. Gibbs, M. Blume, D. Casa, B. Keimer, Y. Murakami, C.-C. Kao, C. Venkataraman, T. Gog, Y. Tomioka, and Y. Tokura, Phys. Rev. B **64**, 195133 (2001).

[17] M. R. Lees, J. Barratt, G. Balakrishnan, D. McK. Paul, and C. Ritter, Phys. Rev. B **58**, 8694 (1998).

[18] Z. Jirác, S. Krupička, Z. Šimša, J. Magn. Magn. Mater. **53**, 153 (1985).

[19] See Supplemental Material at http://link.aps.org/supplemental/10.1103/PhysRevB.91.174405 for an x-ray diffraction characterization of the twin structures of our sample, as well as the T-dependent lattice constants of $Pr_{0.6}Ca_{0.4}MnO_3$.

[20] M. R. Lees, J. Barratt, G. Balakrishnan, D. McK. Paul, and M. Yethiraj, Phys. Rev. B **52**, R14303(R) (1995).

[21] N. Biškup, A. de Andrés, and M. García Hernández, Phys. Rev. B **78**, 184435 (2008).

[22] K. Okada and S. Yamada, Phys. Rev. B **86**, 064430 (2012).

[23] R.-W. Li, H. Wang, X. Wang, X. Z. Yu, Y. Matsui, Z.-H. Cheng, B.-G. Shen, E. W. Plummer, and J. Zhang, Proc. Natl. Acad. Sci. USA **106**, 14224 (2009).

[24] K. Tobe, T. Kimura, and Y. Tokura, Phys. Rev. B **69**, 014407 (2004).

[25] I. V. Solovyev and K. Terakura, Phys. Rev. Lett. **83**, 2825 (1999).

[26] S. Ishihara, J. Inoue, and S. Maekawa, Phys. Rev. B **55**, 8280 (1997).

[27] R. Maezono, S. Ishihara, and N. Nagaosa, Phys. Rev. B **58**, 11583 (1998).

[28] K. L. Kugel and D. I. Khomskii, Sov. Phys. JEPT **52**, 501 (1981).

[29] Q. Yuan and T. Kopp, Phys. Rev. B **65**, 174423 (2002).

[30] R. Kajimoto, T. Kakeshita, Y. Oohara, H. Yoshizawa, Y. Tomioka, and Y. Tokura, Phys. Rev. B **58**, R11837(R) (1998).

[31] Y. Okimoto, Y. Tomioka, Y. Onose, Y. Otsuka, and Y. Tokura, Phys. Rev. B **59**, 7401 (1999).